


ORIGINAL ARTICLE

Open Access



Capacity Contribution Mechanism of rGO for SnO₂/rGO Composite as Anode of Lithium-ion Batteries

Qi Li^{1,2}, Guojun Zhang³, Yuanduo Qu¹, Zihan Zheng¹, Junkai Wang¹, Ming Zhu² and Lianfeng Duan^{1*} 

Abstract

Compared with ordinary graphite anode, SnO₂ possesses higher theoretical specific capacity, rich raw materials and low price. While the severe volume expansion of SnO₂ during lithium-ion extraction/intercalation limits its further application. To solve this problem, in this work the reduced graphene oxide (rGO) was introduced as volume buffer matrix of SnO₂. Herein, SnO₂/rGO composite is obtained through one-step hydrothermal method. Three-dimensional structure of rGO could effectively hinder the polymerization of SnO₂ nanoparticles and provide more lithium storage sites attributed to high specific surface area and density defects. The initial discharge capacity of the composite cathode is 959 mA·h·g⁻¹ and the capacity remained at 300 mA·h·g⁻¹ after 1000 cycles at 1 C. It proved that the rGO added in the anode has a capacity contribution to the lithium-ion battery. It changes the capacity contribution mechanism from diffusion process dominance to surface driven capacitive contribution. Due to the addition of rGO, the anode material gains stable structure and great conductivity.

Keywords: SnO₂/rGO composite, Lithium-ion battery, Capacity contribution, Diffusion coefficients

1 Introduction

Lithium-ion batteries have realized large-scale application in electric and hybrid vehicles. In the past few decades, SnO₂ has attracted extensive attention as electrode material. Compared with ordinary graphite anode materials, SnO₂ possesses higher theoretical specific capacity (790 mA·h·g⁻¹), rich raw materials and low price. While the volume expansion of SnO₂ during lithium-ion extraction/intercalation reaches more than 50%, the high stress caused by volume expansion may lead to the fracture failure of electrode material which makes the specific capacity of the material decrease rapidly, while the rate performance and cycle stability decreasing [1–3]. Therefore, the key to realize the application

of SnO₂ cathode materials in lithium-ion batteries is to find ways to effectively slow down the volume dilatation effect of SnO₂ during the lithium-ion extraction/intercalation process and upgrade the electrochemical performance of electrode materials [4–7]. Graphene is a 2D material with good conductivity and high specific capacity. Graphene nanosheets can not only effectually prevent the volumetric change and particle aggregation of SnO₂, but also improve the conductivity. As an active material for lithium storage, graphene nanosheets keep the structural integrity of electrode [8–10]. Chen et al. synthesize a reduced graphene and SnO₂ nanospheres composite and obtain good performance in the application of lithium-ion batteries or sodium-ion batteries [11]. Zhou et al. built a SnO₂/GO structure by hydrothermal method [12]. It's worth noting that they researched the influence of GO dosage in SnO₂/GO anode and found that the lithium ions storage capability increases with the raise of GO dosage. Lu et al. focused on the drying process after hydrothermal process [13]. By comparing

*Correspondence: lfduan@stu.edu.cn

¹ Department of Chemistry and Key Laboratory for Preparation and Application of Ordered Structural Materials of Guangdong Province, Shantou University, Shantou 515063, China
Full list of author information is available at the end of the article

anodes treated by spray-drying and freeze-drying, novel composition of SnO_2 and GO achieved after spray-drying process obtained favorable lithium-ion transmission during charging/discharging process.

The combination of rGO and anode materials of lithium-ion batteries or sodium-ion batteries can increase the capacitance contribution, which has been confirmed by much research [14–17]. While, for SnO_2 , the influence of rGO on capacitance contribution rate has not been studied. In this work, we report to synthesize SnO_2/rGO composite by the sample single step method. We analyze the lithiation/delithiation process and find that the addition of rGO will significantly improve the mobility of lithium ions. When the scan rate comes to $1 \text{ mV}\cdot\text{s}^{-1}$, the capacitive contribution rate raises from 56% to 71% after the addition of rGO. It confirms that the addition of rGO changes the capacity contribution mechanism from diffusion process dominance to surface driven capacitive contribution dominance attributed to high specific surface area, abundant defects and high conductivity of rGO.

2 Materials and Methods

2.1 Preparation of SnO_2/rGO Composite

The GO dispersion was prepared by the oxidation of graphite powder in acidic environment according to a modified Hummers method [18–20]. The as-obtained aqueous suspension of GO was dispersed under ultrasonication for 6 h and purified with deionized water. In a typical synthesis, 0.904 g (4 mmol) $\text{SnCl}_2 \cdot 2\text{H}_2\text{O}$, 2.3528 g (8 mmol) sodium citrate, 10 ml ethanol and 15 ml GO dispersion ($2 \text{ mg}\cdot\text{mL}^{-1}$) were mixed together to form a uniform solution on a magnetic stirrer. During magnetic stirring, the mixture will be ultrasonically treated for a period of time in order to make the solute fully dispersed. Then the mixture was transferred to a 30 ml reaction kettle for hydrothermal treatment at 180°C for 6 h. Thereafter, the cooled down product was washed by continuous centrifugation method. Finally, the as-obtained product was dried at 60°C for the whole day, the ratio of rGO to SnO_2 is about 4:1. The synthesizing procedure of SnO_2 nanoparticles is just in common with that of SnO_2/rGO in which GO dispersion was replaced by equal amount of deionized water.

2.2 Electrochemical Measurement

CR2025 coin cells were assembled for the following electrochemical investigation. In order to prepare the anode, active materials, conductive carbon black and polyvinylidene difluoride were mixed together to form slurry by 8:1:1. The active material loaded on the Cu foil electrode was about 1.6 mg cm^{-2} . 1 M LiPF_6 in ethylene carbonate was added to dimethyl carbonate (1:1, V/V) as the

electrolyte during the battery assembly process. Constant current charge and discharge test at various rates were performed by LAND CT2001A battery testing system within a voltage range of 0.001–3 V and the electrochemical characterizations were performed by electrochemical workstation (CHI660C, Shanghai).

2.3 Materials Characterization

The microstructure and composition were analyzed by X-ray diffraction (XRD, Rigaku D/max 2500 pc X-ray diffractometer), Fourier transform infrared spectroscopy (FTIR, Nicolet-6700 Thermofisher), Raman spectra (HORIBA Jobin Yvon LabRAM HR800) and X-ray photoelectron spectroscopy (XPS, Thermo Scientific, Waltham, MA, USA). The microstructure was explored by scanning electron microscopy (SEM, JEOL JSM-6700F) and transmission electron microscopy (TEM, FEI, Talos F200). The specific surface area was tested by N_2 adsorption/desorption (NOVA 2000, Quanta chrome).

3 Results and Discussion

For the sake of analyzing the morphology and nanostructure of hydrothermal product, SEM test was carried out on SnO_2 and SnO_2/rGO powders. Figure 1a shows the pure SnO_2 obtained by hydrothermal treatment presents spherical morphology with a diameter of around 1 to 3 microns. Figure 1b illustrates that SnO_2 spheres (with a diameter of approximately $3 \mu\text{m}$) are composed of several spherical nanoflowers with a diameter of about 200 nm.

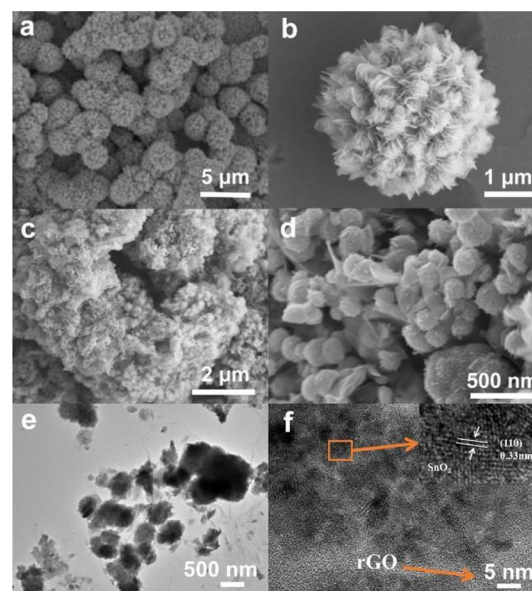


Figure 1 a Low-magnification and b high-magnification of SEM images of SnO_2 nanoparticles, c Low-magnification and d high-magnification of SEM images of SnO_2/rGO composite, e TEM and f HRTEM images of SnO_2/rGO composite

As for SnO_2/rGO (Figure 1c and d), spherical SnO_2 are equably absorbed on the surface of rGO nanosheets, meanwhile the SnO_2 spherical structure remains unchanged. It's obviously that SnO_2 nanoflowers grown on rGO nanosheets, while the size is obviously smaller than that of SnO_2 powders which is about 100 nm. The reduction of the diameter of the nanosphere means the increase of the specific surface area.

TEM spectra (Figure 1e, f) further illustrate the morphology and nanostructure of as prepared materials. It is highly consisted with the results obtained in previous SEM test. SnO_2 nanoparticles are absorbed onto the rGO nanosheets with favorable connection. As for high-resolution TEM spectra (Figure 1f), SnO_2 crystal grains are relatively visible and the rGO nanosheets could be obviously observed and the lattice spacing of 0.33 nm, corresponding to the (110) planes of tetragonal SnO_2 . X-ray diffraction (XRD) is tested for the component analysis of SnO_2/rGO and SnO_2 powder (Figure 2a). As for the XRD spectroscopy of SnO_2/rGO , diffraction peaks in the curve could correspond to that of tetragonal tin dioxide with cassiterite structure (JCPDS Card No.41e1445). While, it's of particular interest that, the XRD spectroscopy of SnO_2 failed to correspond the standard peak one-to-one. This is because the crystallinity of SnO_2 obtained after 6 h of hydrothermal reaction is not high enough, which shifts the peak of 33.8° to the left [22]. Since SnO_2/rGO failed to detect the diffraction peak of rGO, the XRD spectrum results could not prove the existence of rGO.

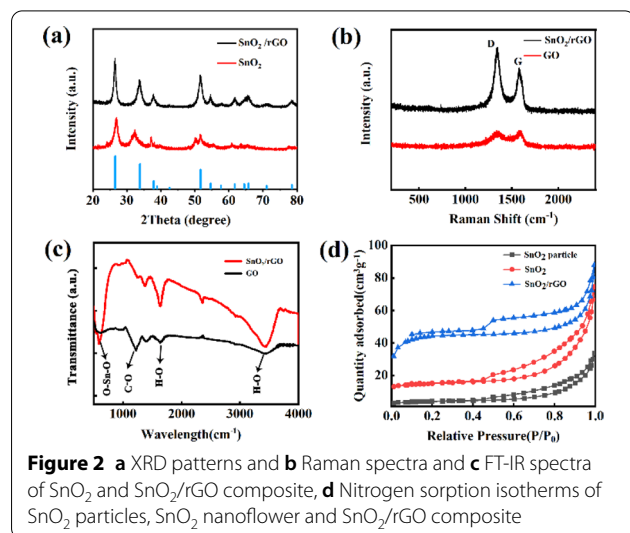
For the common homonuclear diatomic pairs in carbon-based materials, their Raman activity will be strong, so their Raman peaks can be easily detected in Raman spectra, thus the Raman spectroscopy was used for further composition analysis (Figure 2b). There are two

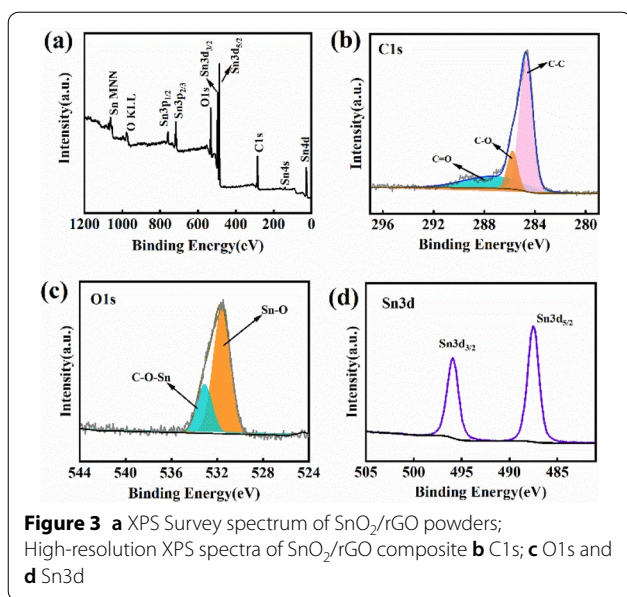
obvious peaks appearing in $\sim 1350\text{ cm}^{-1}$ and $\sim 1580\text{ cm}^{-1}$ corresponding to the D and G bands of graphene respectively. The I_D/I_G significantly increases from 0.98 of GO to 1.76 of SnO_2/rGO , which indicates that the sp^2 domain of SnO_2/rGO composites is smaller. Meanwhile it illustrates that oxygen content of GO reduced during hydrothermal process [21].

In order to further analyze the components and verify the partial reduction of GO during the hydrothermal process. FT-IR spectra of as-prepared nanocomposites are plotted (Figure 2c). Both spectra show the peak of 3440 cm^{-1} and 1629 cm^{-1} which correspond to O-H stretching vibrations of absorbed water molecules and O-H bending vibrations, the absorption band of around 1220 cm^{-1} corresponding to C-O. After compounding with SnO_2 , similar oxygen-containing groups are found in the SnO_2/rGO spectra, which illustrates that GO is partially reduced in hydrothermal treatment, and a strong peak at 669 cm^{-1} is attributed to O-Sn-O stretching mode [22, 23]. N_2 adsorption/desorption test is carried out to analyze the specific surface area of SnO_2 particles (purchase from enterprise), SnO_2 nanoflower and SnO_2/rGO composite in Figure 2d. The BET specific surface area of SnO_2 particles is only $23.16\text{ cm}^2\cdot\text{g}^{-1}$, while it comes to $63.17\text{ cm}^2\cdot\text{g}^{-1}$ when the morphology of SnO_2 turns into spherical nanoflower. As for SnO_2/rGO composite, it reaches $126.74\text{ cm}^2\cdot\text{g}^{-1}$, which is much higher than that of SnO_2 . It illustrates that the assistance of rGO could significantly increase the specific surface area [13]. The larger specific surface area means that SnO_2/rGO can have better contact with electrolyte and absorb more lithium ions at the same time.

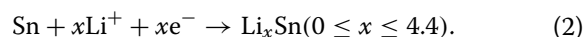
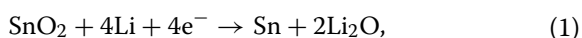
To obtain the exact composition of SnO_2/rGO powders, we tested it with X-ray photoelectron spectroscopy (XPS), since XPS could display the chemical environment of Sn, O and C elements. Figure 3a displays the XPS survey spectra of SnO_2/rGO powders. In C1s fitting patterns (Figure 3b), there are C-C bond at 284.7 eV , C-O bond at 285.6 eV and C=O bond at 286.8 eV , in which C-C bond takes an absolute dominant position. It corresponds to a common rGO chemical bond composition as mentioned in previous study [24]. In O1s spectroscopy (Figure 3c), Sn-O bond at 531.6 eV and C-O-Sn bond at 532.8 eV make different contribution in fitting patterns. The obvious C-O-Sn bond fitting peak indicates that there exists surpassing chemical bonding among SnO_2 and rGO [25]. In Sn3d spectrum (Figure 3d), there are two obvious peaks located at 495.9 eV and 487.6 eV , which correspond to Sn3d 3/2 and Sn3d 5/2 respectively [26]. The peaks generally consist with that reported in pure SnO_2 powder; it illustrates that major constituent of SnO_2/rGO powders is SnO_2 .

For the sake of researching the influence on lithium-ion battery performance after compounding with rGO,





the electrochemical performance tests were carried out. Figure 4a display the initial three cycle cyclic voltammetry (CV) profiles of the electrode which chose SnO₂/rGO composites as active materials in the voltage range from 0.01 to 3.0 V. In the first cycle, the cathodic peak at around 0.78 V could be observed while it disappeared in the subsequent cycles. This situation occurs due to the irreversible reduction of SnO₂ and the formation of solid electrolyte interface (SEI), as described in Eq. (1) [27]. Furthermore, it will lead to significant capacity loss in the first cycle. An obvious reduction peak appeared at the range of 0.08 and 0.13 V, which correspond to the alloying reaction of Sn and Li (Eq. (2)) [28]. Meanwhile it is relevant to the intercalation of lithium [29]. As for the following two cycles, the obvious cathodic peaks at around 1.2 V correspond to the transformation between SnO₂ and Sn [30]. In the charge curve, the anodic peak at around 0.57 V correspond to the reverse process of the alloying reaction mentioned before, which means the decomposition of Li_xSn [31]. There were two weak oxidation peaks at 1.27 and 1.9 V, which corresponded to reversible reaction of SnO₂ and Li₂O. In comparison of the CV curves for the first three cycles, the crest value of alloying/dealloying reaction showed slight decline as cycle number increased, it indicated that SnO₂ nanoparticles brought out further activation during the test period. The CV curves of later cycles had significant overlap ratio, which indicated that SnO₂/rGO has excellent reversibility [28].



When the specific current reaches 0.1 C, the galvanostatic discharge-charge curves of 1st, 2nd, 5th and 10th for the SnO₂/rGO are shown in Figure 4b. In the first cycle, the discharge and charge capacity of the composite are 1114.3 mA·h·g⁻¹ and 731.9 mA·h·g⁻¹, respectively. Compare our study with other SnO₂/rGO materials as the anode for Li ion batteries, the capacitance performance of SnO₂/rGO at 0.1C (1114.3 mA·h·g⁻¹) is superior to SnO₂ NPs/rGO (1100 mA·h·g⁻¹) [11], CGN/SnO₂ composites (1048.7 mA·h·g⁻¹) [32] and SnO₂-RGO (665 mA·h·g⁻¹) [33]. A voltage plateau appears at approximately 1 V in the first cycle, while it can't be observed in the subsequent cycles. It mainly due to irreversible reduction of SnO₂ and electrolyte decomposition. In the following profiles, the voltage plateaus can be observed in the ranges of 0.01–0.5 V and 0.5–1 V corresponding to combination reaction of Li-Sn alloy. These results are highly consistent with the verdicts obtained in previous CV tests.

The cyclic performance and coulombic efficiency of two materials under current density of 0.1 C is displayed in Figure 4c. The initial cycle of SnO₂/rGO galvanostatic discharge-charge give out 959.2 mA·h·g⁻¹ for discharge capacity. In contrast, SnO₂ delivers a discharge capacity of 754.6 mA·h·g⁻¹ with coulombic efficiency of 59.04%. It's obviously that, SnO₂/rGO composite possess much higher discharge capacity and coulombic efficiency than that of SnO₂ nanoparticles. Besides, the decline of discharge capacity with the increase of cycle number for SnO₂/rGO composite is significantly faster than that of SnO₂ nanoparticles. When the cycle number comes to 100, SnO₂/rGO remains discharge capacity of 469.6 mA·h·g⁻¹, and SnO₂ nanoparticles reach to 121.1 mA·h·g⁻¹. The above phenomenon is mainly caused by the following two reasons. Firstly, the SnO₂/rGO composite possess much smaller grain size, which will lead to more active materials participating in the reaction during charge and discharge. Secondly, rGO provides an attached framework for SnO₂. This structure puts out an effective buffer for the volume change in the reaction process. Meanwhile it facilitates the insertion and detachment of lithium ions.

The rate performance of two materials at gradient current densities are displayed in Figure 4d. After 10 cycles charge-discharge process, SnO₂/rGO composite remains capacity of 773.7 mA·h·g⁻¹ at 0.1 C, while SnO₂ nanoparticles come up to 500.9 mA·h·g⁻¹ at the same condition. With rate raising up from 0.1 C to 2 C, rate capability diminishes gradually, moreover, the lithium ions storage capability difference of two materials becomes much

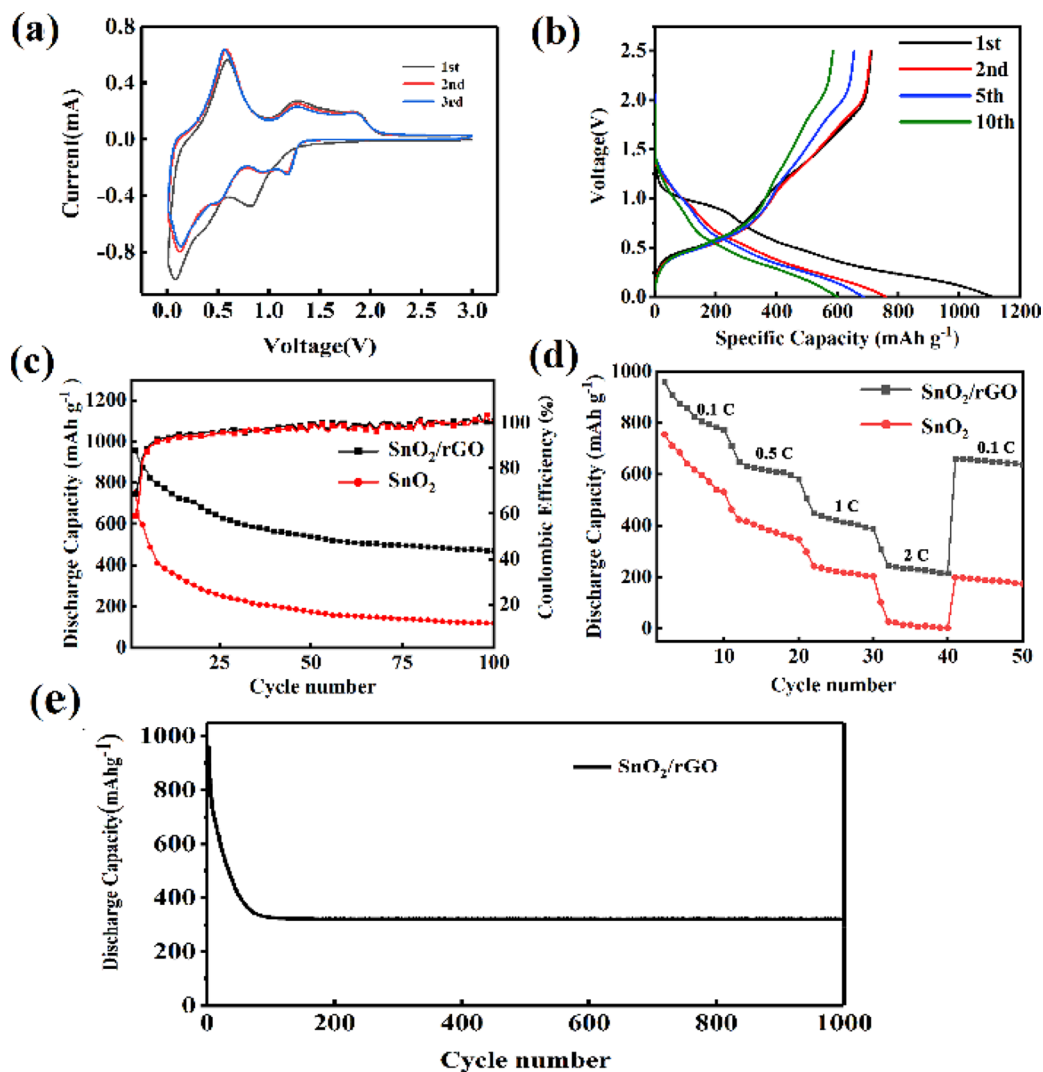
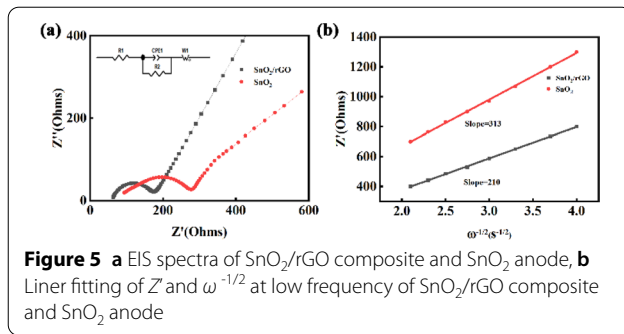


Figure 4 **a** CV curves of SnO_2/rGO composite at a scan rate of $0.1 \text{ mV}\cdot\text{s}^{-1}$, **b** Discharge/charge profiles of SnO_2/rGO composite at different cycles with current rate of 0.1 C , **c** Cycling performance and coulombic efficiency of SnO_2/rGO composite and SnO_2 anode at current rate of 0.1 C , **d** Rate capability of SnO_2/rGO composite and SnO_2 at gradient current rate, **e** Long cycle stability of SnO_2/rGO anode

larger. The reversible capacity of SnO_2/rGO composite come up with $210 \text{ mA}\cdot\text{h}\cdot\text{g}^{-1}$, demonstrating admirable reversible capacity and structure stability under large steady current density [12]. When the rate turns back to 0.1 C , the rate capability of SnO_2/rGO composite is basically restored indicating the great reversible capacity. As for Figure 4e, SnO_2/rGO displays great long-cycle stability even at current charge and discharge rate of 1 C . When the cycle number comes to 1000, the discharge capacity still remains about $300 \text{ mA}\cdot\text{h}\cdot\text{g}^{-1}$. Obviously, the excellent rate performance and cycle stability are attributed to the addition of rGO. It remarkably improves the electrode material stability and provides more lithium ions storage sites [34].

EIS spectra were performed to determine the electrical conductivity and electrochemical kinetics of two electrodes (Figure 5a). The composition of the equivalent circuit was shown above the fitting plot, which can be used for quantitative analysis. A lower charge transfer resistance (R_{ct}) value of SnO_2/rGO composite (65.7 ohms) indicates that the electrode gains better kinetics after introducing rGO into SnO_2 nanoparticles. The reason is that rGO can amend the connections among SnO_2 nanoparticles and present sufficient electronic transmission channels which is favorable for electron transfer [12]. For the sake of further exploring the lithium-ion transfer mechanism, linear fitting of Z' and $\omega^{-1/2}$ at low frequency were carried out in Figure 5b. Lithium-ion diffusion coefficient is a momentous parameter for



evaluating the performance of electrode materials. The following equation is applied to calculate the diffusion coefficients (D_{Li}) of lithium ions (Eq. (3)).

$$D_{Li} = R^2 T^2 / 2A^2 n^4 F^4 C^2 \sigma^2, \quad (3)$$

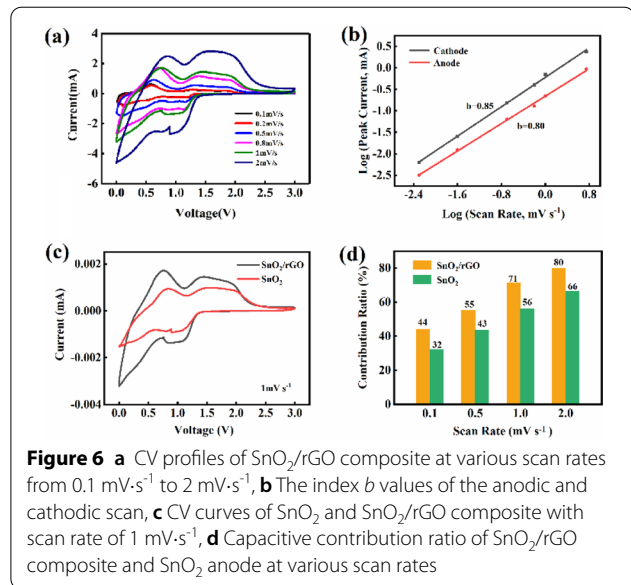
where, R represents gas constant, T stands for Kelvin temperature, A represents the area of electrode, n is the number of electrons transferred during the reaction. F is Faraday constant, σ is the slope of $Z'' \sim \omega^{-1/2}$ and C is lithium-ion phase concentration [35]. From the date in Table 1, we can find that the D_{Li} of SnO₂/rGO electrode is much larger than that of SnO₂. It illustrates that the structure of SnO₂/rGO composite is conducive to the electrolyte diffusion and facilitates Li⁺ migration during lithiation/delithiation process.

The lithium storage kinetics of SnO₂/rGO anode were researched by contrasting CV profiles at different scan rates. By estimating the pseudocapacitive contribution, the high rates performance of SnO₂/rGO anode can be investigated. Meanwhile the influence in complexing rGO in SnO₂ would be further discussed. Figure 6a is the CV profiles of SnO₂/rGO composite under the larger current range as scanning rate raises from 0.1 mV·s⁻¹ to 2 mV·s⁻¹, the capacity contribution mechanism can be expressed by Eq. (4).

$$i = av^b, \quad (4)$$

$$\log(i) = b\log(v) + \log(a), \quad (5)$$

where, b value could be acquired by drawing $\log(i)$ – $\log(v)$ curves and fitting the line to obtain the slope (Eq. 5). Generally, when $b = 0.5$, the capacity contribution is



mainly determined by diffusion process, if $b = 1$, it represents to the typical capacitive charge storage for the surface faradaic redox reaction [36]. The b value obtained from the fitting line of cathodic and anodic peaks are 0.85 and 0.80 for SnO₂/rGO composite in Figure 6b. It indicates that the capacitance contribution of capacitor driving in electrochemical behavior is larger than that of diffusion process for SnO₂/rGO anode. The b value of SnO₂ anode is much closer to 0.5, suggesting that the capacitive contribution is mainly acquired by diffusion process for SnO₂ anode. The significantly higher b value of SnO₂/rGO anode indicates that much larger specific surface area obtained by adding three-dimensional rGO is the main reason for the obvious increase of capacitive contribution. For the sake of investigating the capacity contribution mechanism, total current (I) is separated into two parts by Eqs. (6) and (7).

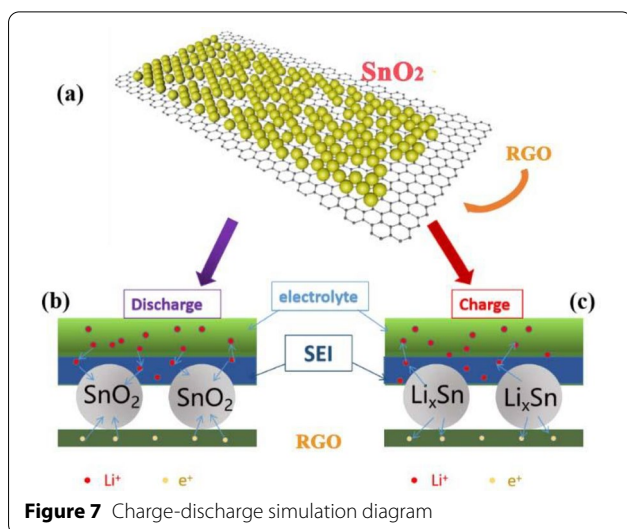
$$I = k_1 v + k_2 v^{1/2}, \quad (6)$$

$$I/v^{1/2} = k_1 v^{1/2} + k, \quad (7)$$

where, $k_1 v$ and $k_2 v^{1/2}$ represents the current attributed to conversion behavior and diffusion-controlled reaction respectively [37]. As shown in Figure 6c and d, when the scan rate comes to 1 mV·s⁻¹, the capacitive contribution of SnO₂/rGO anode is 71%, which is significantly larger than that of SnO₂ anode (56%). This result shows that among two lithium storage mechanisms in SnO₂/rGO anode, the capacitive drive process takes an absolute dominant position owing to large specific surface area [38]. The capacitive contribution gets bigger and bigger in

Table 1 Kinetic parameters of SnO₂/rGO and SnO₂ electrodes

Materials	R_s (Ω)	R_{ct} (Ω)	σ (Ω s ^{-1/2})	D_{Li} (cm ² s ⁻¹)
SnO ₂ /rGO	58.72	65.7	210	1.7×10^{-10}
SnO ₂	85.15	97.4	313	8.5×10^{-11}



the wake of scan rate enlargement as shown in Figure 6d, it is in accord with the charge/discharge profiles and rate performance mentioned before. This result indicates that superior capacitive contribution with large current densities is in favor of clipping Li^+ insertion-extraction reaction [36]. Previous discussions prove that the lithium storage behavior of SnO_2/rGO anode is mainly driven by capacitive behaviors. Meanwhile it is beneficial to cycling stability and rate performance [21]. Besides, it certifies that the structure of rGO could inhibit the aggregation of SnO_2 nanoparticles, which is consistent with the result of SEM.

The charge-discharge mechanism diagram is shown in the Figure 7, and the previous experiments have obtained good electrochemical performance for the following reasons. The addition of rGO provides more loading sites for SnO_2 and can effectively prevent SnO_2 from falling off during the charging and discharging process. rGO has good electrical conductivity, which is conducive to charge transfer. Besides, rGO itself also has the function of storing lithium ions.

4 Conclusions

- (1) In this paper, via a one-step hydrothermal synthesis, graphene was added to SnO_2 to alleviate the volume expansion of SnO_2 in the charging-discharging process of Li ion batteries.
- (2) Taking the advantage of specific surface area, high conductivity and density defects of graphene, the aggregation of SnO_2 can alleviate structurally.
- (3) The capacity contribution mechanism changed from diffusion dominated to surface driven capacitive contribution, which provided more sites for storing lithium ions.

- (4) Even at high current density of 1C and long cycle of 1000 times, the specific capacity of SnO_2/rGO can maintain at $300 \text{ mA} \cdot \text{h} \cdot \text{g}^{-1}$ which has a better practical perspective.

Acknowledgements

The authors sincerely thanks to Professor Fushen Lu of Shantou University and Liying Wang of Changchun University of Technology for their critical discussion and reading during manuscript preparation.

Author contributions

LD was in charge of the whole trial; QL wrote the manuscript; GZ, YQ, ZZ, JW and MZ assisted with sampling and laboratory analyses. All the authors read and approved the final manuscript.

Authors' information

Qi Li, born in 1993, is currently a master candidate at Advanced Institute of Materials Science & Department of Materials Science and Engineering, Changchun University of Technology, China.

Guojun Zhang, born in 1995, is currently a doctoral candidate at SEU-FEI Nano-Pico Center, Key Laboratory of MEMS of Ministry of Education, Southeast University, China.

Yuanduo Qu, born in 1995, is currently a doctoral candidate at Advanced Energy Materials Laboratory, Department of Chemistry, Shantou University, China.

Zihan Zheng, born in 2000, is currently a doctoral candidate at Advanced Energy Materials Laboratory, Department of Chemistry, Shantou University, China.

Junkai Wang, born in 1992, is a lecturer at Advanced Energy Materials Laboratory, Department of Chemistry, Shantou University, China.

Ming Zhu, born in 1997, is currently a master candidate at Advanced Institute of Materials Science & Department of Materials Science and Engineering, Changchun University of Technology, China.

Lianfeng Duan, born in 1981, is currently a Professor at Advanced Energy Materials Laboratory, Department of Chemistry, Shantou University, China. His research interests include new energy materials and devices. Tel: +86-0754-86503795; E-mail: lfduan@stu.edu.cn.

Funding

Supported by National Natural Science Foundation of China (Grant No. 61774022), Natural Science Foundation of Guangdong Province (Grant No. 2022A1515011449), Special Program for Science Research Foundation of the Higher Education Institutions of Guangdong Province (Grant No. 2020ZDZX2052), 2020 Li Ka Shing Foundation Cross-Disciplinary Research Grant (Grant No. 2020LKSG01A), Research. Start-up Foundation of Shantou University (Grant No. NTF20024).

Competing interests

The authors declare no competing financial interests.

Author Details

¹Department of Chemistry and Key Laboratory for Preparation and Application of Ordered Structural Materials of Guangdong Province, Shantou University, Shantou 515063, China. ²Advanced Institute of Materials Science & Department of Materials Science and Engineering, Changchun University of Technology, Changchun 130012, China. ³SEU-FEI Nano-Pico Center, Key Laboratory of MEMS of Ministry of Education, Southeast University, Nanjing 211189, China.

Received: 31 December 2021 Revised: 15 April 2022 Accepted: 22 April 2022

Published online: 03 June 2022

References

- [1] H D Liu, J M Huang, X L Li, et al. SnO_2 nanorods grown on graphite as a high-capacity anode material for lithium ion batteries. *Ceramics International*, 2012, 386 (6): 5145-5149.

- [2] Q H Tian, Y Tian, W Zhang, et al. Impressive lithium storage of SnO_2 @ TiO_2 nanospheres with a yolk-like core derived from self-assembled SnO_2 nanoparticles. *Journal of Alloys and Compounds*, 2017, 70(2): 99-105.
- [3] J Zhang, H Ren, J Y Wang, et al. Engineering of multi-shelled SnO_2 hollow microspheres for highly stable lithium-ion batteries. *Journal of Materials Chemistry A*, 2016, 4(5): 17673-17677.
- [4] J J Liang, C C Yuan, H H Li, et al. Growth of SnO_2 nanoflowers on N-doped carbon nanofibers as anode for Li- and Na-ion batteries. *Nano-Micro Letter*, 2018, 10(2): 1-9.
- [5] N T Wu, W Z Du, X Gao, et al. Hollow SnO_2 nanospheres with oxygen vacancies entrapped by a N-doped graphene network as robust anode materials for lithium-ion batteries. *Nanoscale*, 2018, 10(24): 11460-11466.
- [6] Z C Liu, X H Yuan, S S Zhang, et al. Three-dimensional ordered porous electrode materials for electrochemical energy storage. *NPG Asia Materials*, 2019, 11(1): 1-21.
- [7] X Min, B Sun, S Chen, et al. A textile-based SnO_2 ultra-flexible electrode for lithium-ion batteries. *Energy Storage Materials*, 2019, 1(6): 597-606.
- [8] L B Chen, M Zhang, W F Wei. Graphene-based composites as cathode materials for Lithium ion batteries. *Journal of Nanomaterials*, 2013, 2: 2.
- [9] X L Chen, Y Y Ma. Wearable Lithium ion batteries based on carbon nanotubes and graphene. *Advanced Materials Technologies*, 2018, 3(10): 1800041.
- [10] X Y Chen, Y Tian. Review of graphene in cathode materials for Lithium-ion batteries. *Energy Fuels*, 2021, 35(5): 3572-3580.
- [11] X X Chen, R Z Cai, P G Liu, et al. Preparation and electrochemical performance of reduced graphene and SnO_2 nanospheres composite materials for Lithium-ion batteries and Sodium-ion batteries. *ChemistrySelect*, 2021, 6(13): 3192-3198.
- [12] S Zuo, D Li, Z Wu, et al. SnO_2 /graphene oxide composite material with high rate performance applied in lithium storage capacity. *Electrochimica Acta*, 2018, 264: 61-68.
- [13] Z Y Lu, Z Kong, L Y Jing, et al. Porous SnO_2 /graphene composites as anode materials for Lithium-ion batteries: Morphology control and performance improvement. *Energy Fuels*, 2020, 34(10): 13126-13136.
- [14] D P Cai, B H Qu, Q H Li, et al. Reduced graphene oxide uniformly anchored with ultrafine CoMn_2O_4 nanoparticles as advance anode materials for lithium and sodium storage. *Journal of Alloys and Compounds*, 2017, 716: 30-36.
- [15] S Gupta, N Dimakis. Elucidating the effects of oxygen- and nitrogen-containing functional groups in graphene nanomaterials for applied electrochemistry by density functional theory. *Journal of Applied Physics*, 2021, 130(8): 084902.
- [16] J L Liu, J Wang, C H Xu, et al. Advanced energy storage devices: Basic principles, analytical methods, and rational materials design. *Advanced Science*, 2018, 5(1): 1700322.
- [17] B Quan, A Jin, S H Yu, et al. Solvothermal-derived S-doped graphene as an anode material for Sodium-ion batteries. *Advanced Science*, 2018, 5(5): 1700880.
- [18] L J C Jaemyung Kim, Franklin Kim, Wa Yuan, et al. Graphene oxide sheets at interfaces. *Journal of the American Chemical Society*, 2010, 132(23): 8180-8186.
- [19] K S Novoselov, A K Geim, S V Morozov, et al. Two-dimensional gas of massless dirac fermions in graphene. *Nature*, 2005, 438(7065): 197-200.
- [20] D Wang, J Yang, X Li, et al. Layer by layer assembly of sandwiched graphene/ SnO_2 nanorod/carbon nanostructures with ultrahigh lithium ion storage properties. *Energy Environmental Science*, 2013, 6(10): 2900-2906.
- [21] G Zhang, S Zeng, L Duan, et al. The dual capacity contribution mechanism of SnSb I | anchored nitrogen doped 3D reduced graphene oxide enhances the performance of Sodium ion batteries. *ChemElectroChem*, 2020, 7(22): 4663-4671.
- [22] H J Zhang, Q Q He, X D Zhu, et al. Surfactant-free solution phase synthesis of monodispersed SnO_2 hierarchical nanostructures and gas sensing properties. *Crystengcomm*, 2012, 14(9): 3169-3176.
- [23] S K Park, S H Yu, N Pinna, et al. A facile hydrazine-assisted hydrothermal method for the deposition of monodisperse SnO_2 nanoparticles onto graphene for lithium ion batteries. *Journal of Materials Chemistry*, 2011, 22(6): 2520-2525.
- [24] M Xin, A Bs, C A Shi, et al. A textile-based SnO_2 ultra-flexible electrode for lithium-ion batteries. *Energy Storage Materials*, 2019, 16: 597-606.
- [25] W Yao, S Wu, L Zhan, et al. Two-dimensional porous carbon-coated sandwich-like mesoporous SnO_2 /graphene/mesoporous SnO_2 nanosheets towards high-rate and long cycle life lithium-ion batteries. *Chemical Engineering Journal*, 2019, 6: 234-241.
- [26] S Jiang, R Huang, W Zhu, et al. Free-standing SnO_2 @rGO anode via the anti-solvent-assisted precipitation for superior Lithium storage performance. *Frontiers in Chemistry*, 2019, 7: 878-886.
- [27] H D Bian, Y R Tian, C Lee, et al. Mesoporous SnO_2 nanostructures of ultra-high surface areas by novel anodization. *ACS Applied Materials & Interfaces*, 2016, 8(42): 28862-28871.
- [28] J Lin, Z W Peng, C S Xiang, et al. Graphene nanoribbon and nanostructured SnO_2 composite anodes for Lithium ion batteries. *ACS Nano*, 2013, 7(7): 6001-6006.
- [29] Y J Chao, X X Yuan, Z F Ma. Preparation and characterization of carbon cryogel (CC) and CC-SiO composite as anode material for lithium-ion battery. *Electrochimica Acta*, 2008, 5(39): 3468-3473.
- [30] R Demir-Cakan, Y S Hu, M Antonietti, et al. Facile one-pot synthesis of mesoporous SnO_2 microspheres via nanoparticles assembly and lithium storage properties. *Chemistry of Materials*, 2008, 20(4): 1227-1229.
- [31] R Jia, J L Yue, Q Y Xia, et al. Carbon shelled porous SnO_2 -delta nanosheet arrays as advanced anodes for lithium-ion batteries. *Energy Storage Materials*, 2018, 13: 303-311.
- [32] X Q Zhang, X X Huang, X Geng, et al. Flexible anodes with carbonized cotton covered by graphene/ SnO_2 for advanced lithium-ion batteries. *Journal of Electroanalytical Chemistry*, 2017, 794: 15-22.
- [33] C C Hou, S Brahma, S C Weng, et al. Facile, low temperature synthesis of SnO_2 /reduced graphene oxide nanocomposite as anode material for lithium-ion batteries. *Applied Surface Science*, 2017, 413: 160-168.
- [34] L L Gao, C P Gu, H B Ren, et al. Synthesis of tin(IV) oxide@reduced graphene oxide nanocomposites with superior electrochemical behaviors for lithium-ions batteries. *Electrochimica Acta*, 2018, 290: 72-81.
- [35] C Wang, D Higgins, F F Wang, et al. Controlled synthesis of micro/nano-structured CuO anodes for lithium-ion batteries. *Nano Energy*, 2014, 9: 334-344.
- [36] A Rba, B Gkv, C Sba, et al. Photonic split-second induced mesoporous TiO_2 -Graphene architectures for efficient sodium-ion batteries. *Carbon*, 2021, 178: 332-344.
- [37] T Brezesinski, J Wang, S H Tolbert, et al. Ordered mesoporous alpha- MoO_3 with iso-oriented nanocrystalline walls for thin-film pseudocapacitors. *Nature Materials*, 2010, 9(2): 146-151.
- [38] M Khan, M N Tahir, S F Adil, et al. Graphene based metal and metal oxide nanocomposites: synthesis, properties and their applications. *Journal of Materials Chemistry A*, 2015, 3(37): 18753-18808.

Submit your manuscript to a SpringerOpen[®] journal and benefit from:

- Convenient online submission
- Rigorous peer review
- Open access: articles freely available online
- High visibility within the field
- Retaining the copyright to your article

Submit your next manuscript at ► [springeropen.com](https://www.springeropen.com)